

# Ku-/Ka-Band Extrapolation of the Altimeter Cross Section and Assessment With Jason2/AltiKa Data

Charles-Antoine Guérin, Jean-Christophe Poisson, Fanny Piras, Laiba Amarouche, Jean-Claude Lalaurie

▶ **To cite this version:**

Charles-Antoine Guérin, Jean-Christophe Poisson, Fanny Piras, Laiba Amarouche, Jean-Claude Lalaurie. Ku-/Ka-Band Extrapolation of the Altimeter Cross Section and Assessment With Jason2/AltiKa Data. IEEE Transactions on Geoscience and Remote Sensing, 2017, 55 (10), pp.5679 - 5686. 10.1109/TGRS.2017.2711863 . hal-01731117

**HAL Id: hal-01731117**
**https://amu.hal.science/hal-01731117**

Submitted on 19 Feb 2022

**HAL** is a multi-disciplinary open access archive for the deposit and dissemination of scientific research documents, whether they are published or not. The documents may come from teaching and research institutions in France or abroad, or from public or private research centers.

L'archive ouverte pluridisciplinaire **HAL**, est destinée au dépôt et à la diffusion de documents scientifiques de niveau recherche, publiés ou non, émanant des établissements d'enseignement et de recherche français ou étrangers, des laboratoires publics ou privés.

# Ku/Ka band extrapolation of the altimeter cross-section and assessment with Jason2/AltiKa data

Charles-Antoine Guérin[1] , Jean-Christophe Poisson[2], Fanny Piras[2],
Laiba Amarouche[2] and Jean-Claude Lalaurie[3]
[1] Univ Toulon, Aix Marseille Univ, CNRS/INSU, IRD, MIO UM 110, La Garde, France
[2] Collecte Localisation Satellites (CLS), Toulouse, France
[3] Centre National Etudes Spatiales (CNES), Toulouse, France

***Abstract*—A simple extrapolation technique is proposed for the inter-calibration of Ku and Ka band altimeter data based on a recent analytical scattering model referred to as "GO4". This method is tested with AltiKa and Jason2-Ku altimeters using one year of reprocessed data with the improved retracking algorithm ICENEW. The variations of the normalized radar cross-section with respect to the main oceanic parameters are investigated in Ku and Ka band; the latter band is shown to have an increased sensitivity to wind speed, significant wave height as well as sea surface temperature. As a by-product of this analysis we derive an original expression for the swell impact on the mean square slope which allows to correct the GO4 model for the contribution of long waves. We show that the Ku/Ka prediction agree within 0.25 dB with the respective levels of AltiKa and Jason2-Ku cross-sections at wind speed larger than 4 m/s.**

## I. Introduction

The use of the Ka band (35 GHz) for altimeter measurements has attracted growing interest in the last years as it allows for reduced dimensions of on board instruments as well as a significant improvement of resolution and accuracy in the estimation of the sea surface topography. The first Ka-band nadir altimeter ever used in oceanography is the AltiKa instrument, which was launched with the French-Indian SARAL (Satellite for ARgos and ALtiKa) satellite in February 2013 (see e.g. [1] for an overview of the mission). The results and performances of the AltiKa mission have been well documented already after one year of operation (see for instance the special issue [2]). AltiKa products (wind speed, sea surface height, significant wave height) have been assessed by colocation with other altimeters working in the conventional Ku band as well as buoys ([3], [4], [5], [6], [7], [8], [9], [10]) and have shown excellent overall data quality.

While, however, the dependence on the oceanic conditions of the Ku-band backscatter coefficient ($\sigma^0$) is by now well-established, there has been only few models and measurements in Ka band (see for instance [11] and references therein) to characterize the sea surface response to electromagnetic waves at millimeter wavelength. The use of such a high frequency raises new issues related to the physical description of the resonant surface waves (parasitic capillary waves) or the atmospheric attenuation. There is therefore a need for assessment of both the calibration and the sea state dependence of the Ka band $\sigma^0$. The main objective of this paper is to propose and assess an extrapolation method to infer the sea state dependence of the Ka-band NRCS from the Ku-band counterpart, for which many years of measurement are available. To do this we take advantage of some general theoretical constraints linking the $\sigma^0$ measured at neighboring radar frequencies to establish sharp bounds on the Ka-band $\sigma^0$, given the Ku-band $\sigma^0$. This extrapolation from Ku- to Ka-band values is made possible by a recent, tractable backscattering model referred to as the GO4 model ([12]). To parametrize the model, we use some findings of [13] based on the analysis of the recently launched Ku/Ka Global Precipitation Measurement (GPM) radar, which allows to identify the short-wave contribution to the mss at different cut-off scales. The assessment of this method relies on a systematic study of one year of data from the Ku-band altimeter Jason2 and the recent Ka-band altimeter AltiKa. Even through the absolute calibration of these instruments is not expected to be better than 1 dB, their relative calibration is known to be quite consistent due to similar design and the choice of space agencies to take the historical 30 years of existing Ku altimeter data as a reference value. Our main finding is the full consistency (within 0.25 dB) of the Ku/Ka extrapolation method with the AltiKa/Jason-

2 data sets at moderate and large wind speeds (above 4 m/s) and a less accurate but still satisfactory prediction at smaller wind speeds. As a by-product of this analysis we obtain a simple expression of the mean contribution of long waves to the mean square slope, thereby correcting the celebrated Cox and Munk wind dependence by a further dependence on the significant wave height. The paper is organized as follows. The GO4 scattering model and the Ku/Ka extrapolation technique are introduced in Section II. The data sets and processing techniques are presented in Section III and a systematic comparison of the evolution of the Ku and Ka band NRCS with the oceanic parameters is performed in Section IV. The extrapolation technique is evaluated in Section V.

## II. Theoretical background for Ku/Ka band extrapolation

The GO4 model ([12]) is a simple and accurate model to describe the Normalized Radar Cross-Section (NRCS, $\sigma^0$) at near-nadir incidence angles, except at small wind speed. It is an improvement of the classical Geometrical Optics model (GO2) with an extra term taking into account the surface curvature and the finite radar wavelength. It recovers the reference method, namely the Physical Optics, in the angular domain where the latter is valid. At nadir where azimuthal effects are negligible, the isotropic version of the model can be used to evaluate the NRCS. For small incidence angle $\theta$ (measured from the vertical), the isotropic GO4 approximation writes:

$$\sigma^0 = \sigma^0_{GO2}\left[1 + \frac{\mathrm{msc}\left(2 - 4\frac{\tan^2\theta}{\mathrm{mss}} + \frac{\tan^4\theta}{\mathrm{mss}^2}\right)}{16K^2\mathrm{mss}^2\cos^2\theta}\right], \quad (1)$$

where $K$ is the electromagnetic wavenumber and the first term is the GO2 factor:

$$\sigma^0_{GO2} = \frac{|R|^2}{\mathrm{mss}}\sec^4\theta\exp\left(-\frac{\tan^2\theta}{\mathrm{mss}}\right), \quad (2)$$

with $|R|^2$ the reflectivity factor related to the Fresnel reflection coefficient. Here $\mathrm{mss}$ is the total mean square slope of the sea surface and $\mathrm{msc}$ is the effective mean square curvature as described in [12]. The GO4 formulation reduces the required knowledge of the sea spectrum to two parameters only, namely the mss and msc, and incorporates non-Gaussian deviations of the sea surface statistics in the effective curvature. Only the latter quantity is dependent on the radar frequency. The mss and msc are simply related to the value of the NRCS at nadir ($\theta = 0$) through:

$$\sigma^0 = \frac{|R|^2}{\mathrm{mss}}\left(1 + \frac{\mathrm{msc}}{8K^2\mathrm{mss}^2}\right) \quad (3)$$

As seen, the curvature correction explains the needs for the "radar-filtered" $\overline{\mathrm{mss}} < \mathrm{mss}$ which is often employed to improve the accuracy of the classical GO2 model and can be identified with:

$$\overline{\mathrm{mss}} = \mathrm{mss}\left(1 + \frac{\mathrm{msc}}{8K^2\mathrm{mss}^2}\right)^{-1} \quad (4)$$

The mss and msc parameter cannot be jointly identified with the sole value of the nadir NRCS. However, if a reliable estimate of the mss is known, the relation (3) can be inverted to give the msc parameter:

$$\mathrm{msc} = \frac{8K^2\mathrm{mss}^2}{|R|^2}\left(\mathrm{mss}\ \sigma^0 - |R|^2\right) \quad (5)$$

A first, simple relationship between the NRCS at different bands can be obtained by using the simple fact that the msc is a growing function of frequency, hence larger in Ka band than in Ku band:

$$\mathrm{msc}_a > \mathrm{msc}_u \quad (6)$$

This gives the following lower bound for the Ka band NRCS:

$$\sigma^0_a > \left|\frac{R_a}{R_u}\right|^2\left(\frac{K_u}{K_a}\right)^2\sigma^0_u + \frac{|R_a|^2}{\mathrm{mss}}\left(\frac{K_a^2 - K_u^2}{K_a^2}\right)) \quad (7)$$

where we have denoted with a subscript $u$ or $a$ any quantity associated to the Ku or Ka band, respectively. To obtain an upper bound for the Ka band NRCS, an estimation of the msc is necessary. For this we use the definition which was proposed in [12] for the msc at a given radar frequency:

$$\mathrm{msc} \simeq \int_{|k|<K} d\boldsymbol{k}\ k^4\Psi(\boldsymbol{k}) + \frac{8}{3}\lambda_4\mathrm{mss}^2K^2, \quad (8)$$

where $\Psi$ is the sea surface wave number spectrum and $\lambda_4 \simeq 0.4$ the excess kurtosis of slopes. It is thus composed of the geometrical curvature of waves smaller than the EM wavelength, augmented with a term related to the peakedness of waves. This implies the following upper bound:

$$\begin{aligned}\mathrm{msc}_a = &\left(\int_{|k|<K_u} d\boldsymbol{k}\ k^4\Psi(\boldsymbol{k}) + \frac{8}{3}\lambda_4\mathrm{mss}^2K_u^2\right)\\ &+ K_a^2\int_{K_u<|k|<K_a} d\boldsymbol{k}\ k^2\Psi(\boldsymbol{k}) + \frac{8}{3}\lambda_4\mathrm{mss}^2(K_a^2 - K_u^2)\end{aligned} \quad (9)$$

The first parenthesis on the right-hand side is the Ku band curvature, $\mathrm{msc}_u$. The second term is proportional to the increase of radar-filtered mss from Ku to Ka band,

$$\int_{K_u<|k|<K_a} d\boldsymbol{k}\ k^2\Psi(\boldsymbol{k}) = \overline{\mathrm{mss}}_a - \overline{\mathrm{mss}}_u \quad (10)$$

Hence,

$$\mathrm{msc}_a \leq \mathrm{msc}_u + K_a^2(\overline{\mathrm{mss}}_a - \overline{\mathrm{mss}}_u) + \frac{8}{3}\lambda_4 \mathrm{mss}^2(K_a^2 - K_u^2) \tag{11}$$

yielding after some calculations

$$\sigma_a^0 < \left|\frac{R_a}{R_u}\right|^2 \left(\frac{K_u}{K_a}\right)^2 \sigma_u^0 + \frac{\left|R_a^2\right|}{\mathrm{mss}} \left(1 + \frac{\lambda_4}{3}\right) \left(\frac{K_a^2 - K_u^2}{K_a^2}\right) + \left|R_a^2\right| \frac{\overline{\mathrm{mss}}_a - \overline{\mathrm{mss}}_u}{8\mathrm{mss}^3} \tag{12}$$

The inequalities (7) and (12) give tight bounds for the estimation of the Ka band NRCS given the Ku band NRCS, provided the sea surface mss and the augmentation of the radar-filtered mss are accurately known. We will see in upcoming sections how these quantities can be parametrized.

## III. Processing of the AltiKa and Jason-2 data set

The Ku/Ka extrapolation technique has been applied to Jason-2/AltiKa data using consistent retracking algorithms, as described below.

### *A. The retracking algorithm*

In satellite radar altimetry, the backscatter coefficient is estimated through the retracking of radar waveforms. This processing consists in fitting a waveform model to the returned radar echo acquired by the altimeter. In the ground segment of Low Resolution Mode altimetry missions such as Jason-2 and SARAL/AltiKa, Maximum Likelihood Estimators (MLE) based retrackers are used to retrieve geophysical estimates ([14]). These ocean-dedicated algorithms are based on the Brown model denoted here $S(t)$ ([15], [16]), $t$ being the time. It is defined by the convolution of 3 terms:

$$S(t) = (FSSR * PDF * IR)(t), \tag{13}$$

where $FSSR$ is the average flat sea surface response, $PDF$ is related to the surface elevation probability density of scattering elements and $IR$ is the altimeter impulse response. In the Brown model ([15], [16], [14], the sea surface is considered homogeneous and the NRCS constant in the antenna footprint. In that case, the trailing edge slope variations are only impacted by the platform pointing angle. At the same time the maximum received power is influenced by the platform mispointing. Consequently, the MLE-4 retracker (four parameters retracker) used operationally for Jason-2 and SARAL/AltiKa missions ([14]) is able to correct the NRCS from this platform effect using the trailing edge slope value. However, in some cases, the trailing edge is also affected by inhomogeneous or very low values of surface roughness or sometimes by atmospheric perturbations such as rain cells. Unfortunately, in such situations, the Brown model is not able to distinguish between the platform and surface effects on the trailing edge which can directly affect the NRCS estimation from the MLE-4 retracker. Indeed, it has been shown by [17] and [18] that, in the case of non platform mispointing, the NRCS estimated by the MLE-4 is directly correlated to the slope of the waveform trailing edge which is interpreted as a mispointing by the retracker. The estimated NRCS is therefore directly impacted by trailing edge perturbations since variations of the NRCS in the antenna footprint have been ignored in the FSSR term in (13) ([15], [16]).

Ka band is more impacted by atmospheric perturbations than Ku band. At the same time, Jason-2 and AltiKa platforms showed very low platform mispointings. In this context, MLE-4 backscatter coefficient estimates cannot be considered for the NRCS cross-comparison between Jason-2 and AltiKa measurements since MLE-4 estimates will be degraded by surface roughness effects. A new retracker called ICENEW ([18], [19]) has been used to process 1 year of Jason-2 (Ku and C) and AltiKa data. This new algorithm was originally developed for sea ice and ice sheets region and then applied to process data affected by rain cells and sigma blooms, and also altimeter data acquired over hydrological areas. This retracking introduces the mean square slope of the surface in the Brown model to account for NRCS variations in the antenna footprint. Consequently, the resulting model allows the retracker to decorrelate the NRCS estimate from the slope of the trailing edge and thus provides a more physical value of the NRCS which is crucial for ocean backscatter coefficient cross-comparison. As for the previous models ([15], [16], [14], the ICENEW model is based on the radar equation and on the convolution of the three terms as in equation (13) above. However, contrary to the aforementioned models that considered a constant NRCS in the antenna footprint, the ICENEW model uses a more realistic NRCS value that depends on the incidence angle and the surface mean square slope (mss) as follows:

$$\sigma^0(\theta) = \sigma^0(0)\exp(-\sin^2\theta/\mathrm{mss}) \tag{14}$$

Including this new NRCS formulation in the three terms convolution of equation (13) leads to a new waveform analytical formulation. However, the new analytical formulas can still be written in a manner very close to the existing Brown models. Using the same notation as in

[14], the ICENEW model can be expressed as:

$$S(t) \sim \exp(-\alpha\left(t - \frac{\alpha\sigma_c^2}{2}\right))(1 + \mathrm{Erf}\left(\frac{t - \alpha\sigma_c^2}{\sqrt{2}\sigma_c}\right)), \tag{15}$$

where $\alpha = \delta - \beta^2/4$, $\delta = 4c/(\Gamma h)\ \cos(2\xi)$, $\beta = 4\sqrt{c}\sin(2\xi)/(\Gamma\sqrt{h})$, $\sigma_c$ is related to the SWH and to the shape of the altimeter range impulse response, $c$ is the speed of light, $\xi$ is the off-nadir pointing angle and $h$ is the modified satellite altitude given by $h = H(1+H/R)$, with $H$ the satellite altitude and $R$ is the Earth radius. $\Gamma$ is the main new term introduced in ICENEW given by:

$$\Gamma = \frac{4\gamma \mathrm{mss}}{4\mathrm{mss} + \gamma}, \tag{16}$$

where $\gamma$ is the antenna beamwidth parameter given by $\gamma = \frac{1}{2}\ln(2)\sin^2(\theta_{3dB})$ ($\theta_{3dB}$ being the half-power antenna beamwidth). Typical improvements brought by the ICENEW retracker for the NRCS estimate are shown in Figure 1. AltiKa waveforms are presented in a 2D view and are corrected from the altimeter Automatic Gain Control in order to represent the actual power variation of the return signal in the waveform amplitude. The segment was chosen because AltiKa has overflown a rain cell between latitudes 3.22 and 3.34. The rain impact is clearly visible on Ka echoes in spite of a strong attenuation of the signal amplitude which has been divided by 2. At the bottom, the corresponding backscatter coefficient estimates are plotted in output of the ICENEW and the MLE-4 algorithms. The difference between the two algorithms is significant and can be as large as 1 dB in the middle of the rain cell (latitude 3.275). The ICENEW NRCS estimate shows a decrease of about 3 dB consistent with the waveform amplitude in the top figure, which is not the case for the MLE-4 estimate. Another method has been used in [18] to correct the MLE-4 NRCS from the unwanted effects of the waveform trailing edge perturbations. This method is based on an empirical solution using the trailing edge slope and the pointing angle and has been found to be very consistent with the ICENEW retracker. A systematic comparison (not shown here) of the $\sigma^0$ estimates derived from the two methods using the one-year Jason-2 Ku data set yields a quasi-perfect linear relationship $y = Ax + B$ with coefficients $A = 1.001$ and $B = 0.011$. In the present work, we made the choice to use the ICENEW retracker in order to apply a robust and physical solution to Ku and Ka bands with no further empirical adjustment.

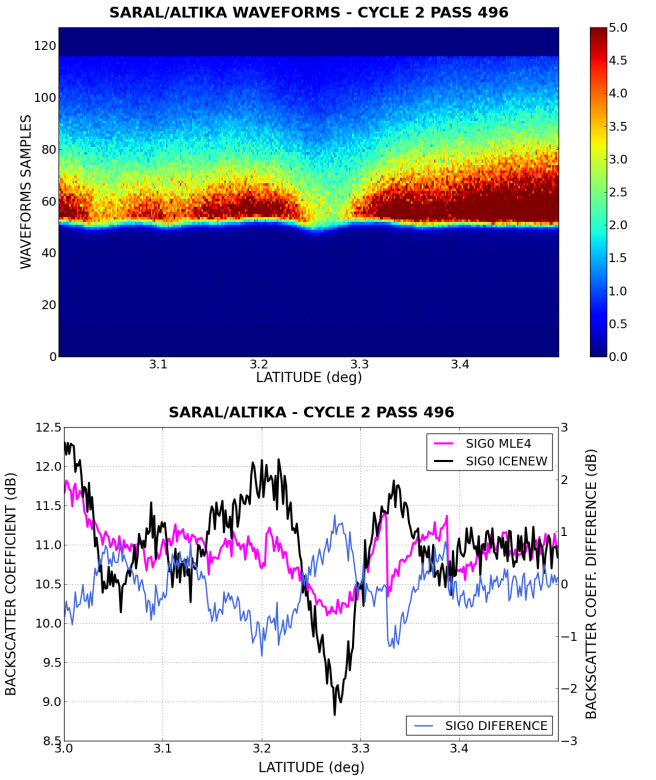



**Fig. 1:** Top figure: AltiKa waveforms corrected from the altimeter Automatic Gain Control represented in 2D: the X-axis is the latitude and Y-axis the waveform bin number. Bottom figure: comparison between along-track ICENEW $\sigma^0$ estimate in black, MLE-4 $\sigma^0$ estimate in magenta and the difference in blue. The $\sigma^0$ difference can be read on the right Y axis.

### *B. Data selection and editing*

In this study, we used 20 Hz Jason-2 data in Ku band from SGDR products ([19]) extended with additional parameters computed in the frame of the CNES PISTACH project ([20]). One year of Jason-2 data has been selected from June $20^{th}$, 2013 to July $22^{nd}$, 2014 (cycles 183 to 222). For the Ka band we have considered 40 Hz AltiKa data from CNES value added PEACHI products ([21], [22]) from June $27^{th}$, 2016 to July $17^{th}$, 2014 (cycles 4 to 14). This period has been chosen to avoid the first AltiKa cycles where numerous platform maneuvers have been performed and to avoid SARAL mispointing issues which occurred in late summer 2014. The ICENEW retracker has been applied to both the Ku and Ka band missions and the Significant Wave Height (SWH) and the NRCS have been evaluated. The output estimates have been compressed to a 1 Hz rate in order to correct them from atmospheric perturbations derived from radiometer measurements. The wind speed at ten meter above the sea surface ($U_{10}$) is also provided in the altimetry products for both missions. However, we found it preferable in our analysis not to use these values as they are related to the backscatter coefficient under assessment. For the sake of consistency, the wind speed values have instead been extracted from the ECMWF

model interpolated on the two mission orbits.

A specific editing has been implemented to be able to compare and characterize altimeter data associated to these two different missions and three frequency bands. A first step is the selection of ocean data by combining the surface type flag (for removing land data), the ice flag and a latitude restriction between $\pm 60°$ (for removing sea ice). To eliminate the possible influence of the additional fetch parameter, radar cells located at less than 200 km from the coast have been discarded. As such a large fetch, we may reasonably assume the sea state to be fully developed for a large proportion of data, even through we have no indication on how long wind has been blowing. Then a quality editing has been applied to remove retracking errors and/or polluted data (by atmospheric events or surface heterogeneities) using Cal/Val criteria defined in [23] and [24], respectively, for Jason-2 and SARAL/AltiKa data. It should be noted that the retracking quality has been accounted for during the compression step (the step that builds 1 Hz data) where a criterion has been applied on the mean quadratic error between the retracked model and the radar echo.

## IV. Jason-2/AltiKa comparison

Figure 2 shows the probability density function of $\sigma^0$ (in dB) over one year for the two radar frequencies, regardless of the oceanic conditions. The mean value of the NRCS is found to be $\sigma^0 = 11.14$ dB in Ka band and $\sigma^0 = 13.65$ dB in Ku band with standard deviations 2.09 dB and 1.83 dB, respectively. A clear evolution of the distribution with the radar frequency is visible. As expected, the central value decreases as the radar frequency is increased (with a mean difference of 2.5 dB) , which is consistent with the fact that the surface is rougher at smaller EM wavelength. The dispersion of the NRCS about its mean value augments with the radar frequency. This is related to the increased dynamical range undergone by the Ka band NRCS as the main oceanic parameters vary (see Section IV).

The dispersion of the NRCS in different bands is known to be due to the variability of wind and waves conditions (e.g., [25], [26], [27]). Wind speed is the dominant parameter while SWH is a secondary parameter which becomes increasingly important at low wind speed. Figure 3 shows the evolution of the mean NRCS for a given wind speed $U_{10}$ as well as the mean NRCS for a given SWH at small wind speed ($U_{10} < 3$ m/s), for both the AltiKa and Jason2-Ku band data sets. The Ka band NRCS shows an enhanced sensitivity to wind speed (especially at low wind speed) with an increased dynamical range with respect to the Ku band NRCS (9 dB versus 7 dB). As small wind speed, a larger

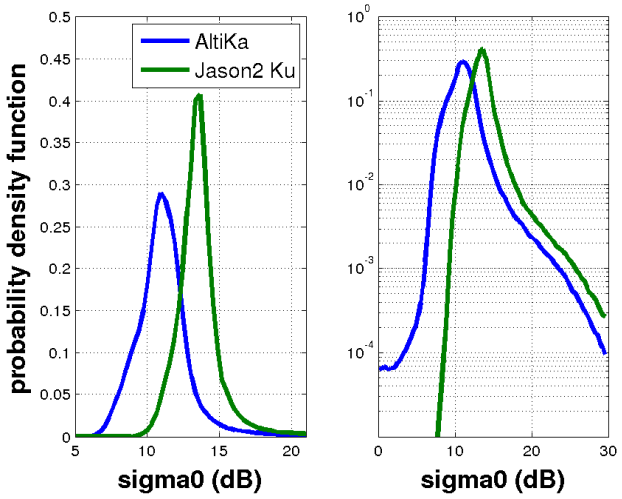



**Fig. 2:** Distribution of the NRCS (in dB values) for the Ku- and Ka-bands after dedicated data selection and editing. The Ku-band $\sigma^0$ are taken from reprocessed Jason-2 measurements and the Ka-band $\sigma^0$ from reprocessed SARAL/AltiKa measurements. The probability density function is given in linear scale on the left panel and semi-log scale on the right panel.

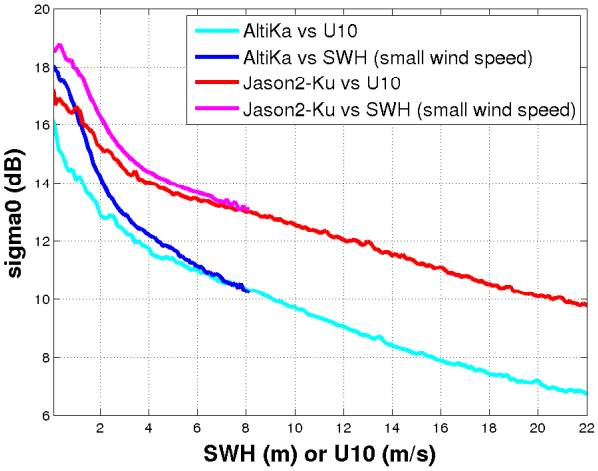



**Fig. 3:** Mean AltiKa and Jason-2 Ku NRCS as a function of wind speed alone or as a function of SWH, averaged over small wind speeds ($U_{10} < 3$ m/s). The plots share the same x-axis, which indicates either $U_{10}$ or SWH values.

sensitivity to the SWH is also found in the Ka-band, with a dynamical range of 8 dB versus 6 dB for the Ku band counterpart.

In earlier works [25], [26], [27] it was found that the use of dual frequency makes it possible to diminish the sea state dependence in the NRCS and helps improving the wind speed estimation. This is confirmed by Figure 4, which displays the difference (in dB) between the Ku-band and Ka-band mean NRCS $((\sigma^0_u)_{dB} - (\sigma^0_a)_{dB})$ in the wind-wave diagram. This NRCS variation has

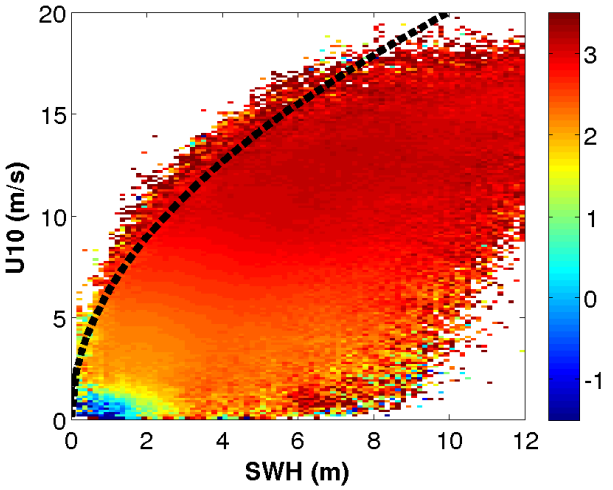



**Fig. 4:** Difference (in dB) between the Ku- and Ka-band mean NRCS. The Pierson-Moskowitz relationship SWH $= 0.025\ U_{10}^2$ for fully developed seas is shown in dashed black lines and limits the available SWH $- U_{10}$ domain.

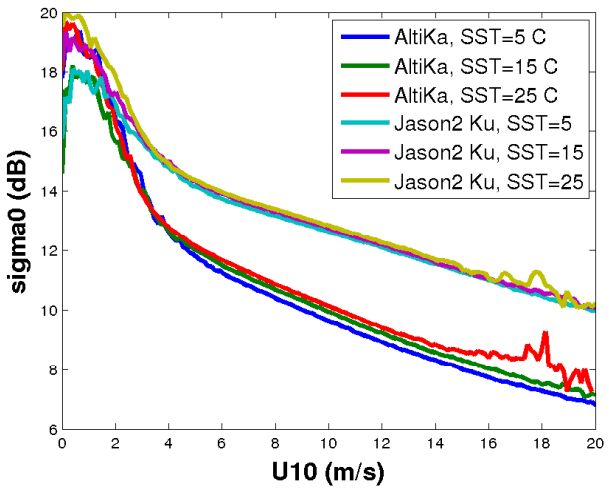



**Fig. 5:** Wind speed dependency of the reprocessed $\sigma^0$ in Ku and Ka bands for 3 different SST values: 5°C, 15°C and 25°C.

indeed little dependence on SWH and increases with wind speed.

To make a consistent comparison of the NRCS measured at different frequencies and eliminate discrepancies which could be due to different sea states, we have computed the $\sigma^0$ difference at crossovers points between Jason-2 Ku and AltiKa. Such a comparison has already been performed over 15 months of mission in [5]. However, this analysis will be redone in the present context with a consistent use of the IceNew retracking for the two datasets. The crossovers should be computed with a short time lag between the two satellites to avoid differences due to the evolution of sea state. Since, however, the number of selected crossover points is dramatically reduced as a stringent constraint on the time lag is imposed, a compromise must be found. A sufficient number of crossover points should be available in order to have a statistically representative result while the maximum authorized time lag should be short at the scale of the sea state variations. We found this optimal value of the maximum time lag to be about 30 minutes, where 1627 crossover points could be selected and well distributed over oceans. As expected the difference between Ka and Ku bands NRCS has be found higher at high latitudes where wind speeds are in general stronger. We found a quasi-linear increase of the Ku/Ka NRCS offset, from about 2.2 dB at the smallest wind speeds to about 3.1 dB at 15 m/s. This is consistent with the findings of [5] (his Figure 2d) who found an increasing offset from about 2.3 dB at small wind speed to 3.2 dB at large wind speed.

It has been recently observed ([28]) that the SST can have an important impact on the NRCS level in Ka band, contrarily to the more conventional Ku band. In order to highlight this dependency in the reprocessed data set, we have interpolated the Reynolds sea surface temperature (SST) ([29]) data to Jason-2 and AltiKa measurement time-tag. The $\sigma^0$ wind speed dependency has then been recalculated for 3 different SST values: 5°C, 15°C and 25°C in both Ka and Ku bands. The result is plotted on Figure 5. The impact of SST is clearly visible on the Ka band (red curves) where the differences between 5°C and 25°C curves can reach up to ∼0.5 dB while the Ku band (blue curves) is almost not affected.When averaged over all available wind speeds and sea states, the difference between the Ku- and Ka-band NRCS is found to vary by ∼0.7 dB, from 3 dB at 0°C to 2.3 dB at 30°. This is consistent with the findings of [28].

## V. Assessment of the Ku/Ka extrapolation

We will evaluate the GO4 extrapolation formulas (7) and (12) in the light of the combined Jason2 and AltiKa data sets. Even though the variations of NRCS caused by SWH are much smaller than those due to wind speed, they are far from being negligible and it is important to incorporate them in the analysis, that is to correct the GO4 model with an extra SWH parameter. To do this, we assume that the sea surface at a given wind speed is described by a superposition of wind-generated waves and a swell component with mean square slope $\mathrm{mss}_{sh}$ and $\mathrm{mss}_l$, respectively (the subscript "sh" and "l" standing for short- and long-waves), so that the total mean square slope is $\mathrm{mss} = \mathrm{mss}_l + \mathrm{mss}_{sh}$. We further assume that the long waves do not significantly modify

the effective msc, which is dominantly affected by short waves. On differentiating the GO2 formula (2) with respect to the mss parameter we obtain the variation of NRCS $\Delta\sigma^0$ induced by an extra long wave component in the mean square slope, $\mathrm{mss}_l$.

$$\frac{\Delta\sigma^0}{\sigma_0} = -\frac{\mathrm{mss}_l}{\mathrm{mss}_l + \mathrm{mss}_{sh}} \tag{17}$$

The resulting variation in dB is $10\log_{10}(\sigma_0 + \Delta\sigma^0) - 10\log_{10}(\sigma_0)$, that is:

$$(\Delta\sigma^0)^{dB} = 10\log_{10}\left(\frac{\mathrm{mss}_{sh}}{\mathrm{mss}_l + \mathrm{mss}_{sh}}\right) \tag{18}$$

Note that this bias is independent on the radar frequency at this level of approximation. This is consistent with the observation of Figure 3 with the aforementioned limitations. For developed wind seas, the mss as a function of wind speed at 12.5 m above the sea surface $U_{12.5}$ is given by the well-known Cox and Munk (CM) relationship ([30]).

$$\mathrm{mss} = 0.003 + 0.0052\ U_{12.5} \tag{19}$$

Note that this relation depends on the sole wind speed parameter and is therefore averaged over possible SWH. The offset $0.003$ in this relation can thus be considered as the mean contribution of swell to the mss, so that $\mathrm{mss}_{sh} = 0.0052\ U_{12.5}$. To incorporate the explicit dependence of the total mss on the SWH, we assume a simple linear relationship $\mathrm{mss}_l = \alpha$ SWH. The coefficient $\alpha$ is found by requiring that the NRCS at a given wind speed, once corrected for the long wave bias (18), is independent on the SWH. With an empirical investigation of the AltiKa and Jason2 data binned by wind speed and SWH, we found the following estimation for the SWH dependence of the swell mss:

$$\mathrm{mss}_l = 0.003\ \mathrm{SWH} \tag{20}$$

so that the total mss has the following joint dependency to the wind and SWH parameters:

$$\mathrm{mss} = 0.0052\ U_{12.5} + 0.003\ \mathrm{SWH} \tag{21}$$

The simplifying assumption than the msc does not depend on long waves might break down at low wind speed, where the relative contribution of long wave to the fourth moment of the wave spectrum (eq. (8)) might be non-negligible with respect to the wind-wave contribution. Hence we do not except the simple relation (21) to hold at the lowest wind speeds. Figures 6 show the Altika as a function of wind speed for different SWH (set of red curves). Once the swell-induced bias $(\Delta\sigma^0)^{dB}$ has been substracted, the different plots collapse to a single plot with little dispersion, except at small wind speed for the aforementioned reason. A very similar pattern is observed for Jason2 NRCS.

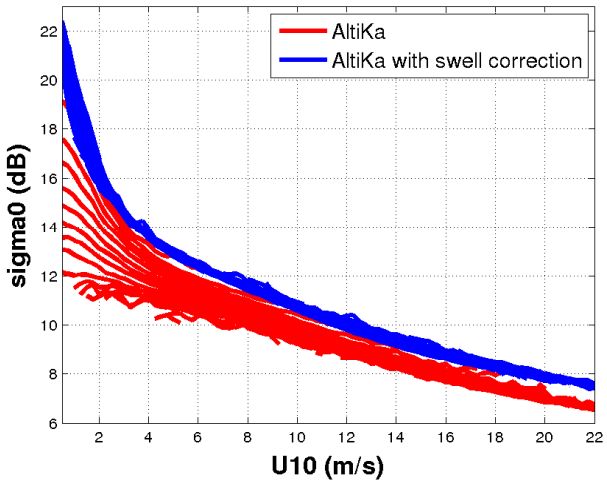



**Fig. 6:** AltiKa NRCS binned by SWH (from 0.5 to 14 m) as a function of wind speed (solid red lines). Once detrended from the swell effect (18), the different plots practically merge together (dashed blue line)

The mss as been evaluated as a function of both wind speed and SWH using the improved formula (21) and converting the $U_{10}$ value in $U_{12.5}$ value by means of a standard von Karman logarithmic profile. The variation of radar-mss from Ku to Ka band has been recently estimated with help of the dual-frequency GPM data ([13], figure 4 ) with the following estimate:

$$\overline{\mathrm{mss}}_a - \overline{\mathrm{mss}}_u = 5.8e-5\ (U_{10} - 1.9)^2 + 7.5e-4 \tag{22}$$

Note that this radar-filtered mss correspond to the mss shape parameter in the angular fit of the scattering diagram and is therefore free of calibration issues. The complex permittivity entering in the reflectivity has been calculated with the modern model by [31] using a mean value of 15 degree Celsius for the SST and 35 PSU for the salinity. The corresponding bounds (7) and( 12) for the Ka band NRCS have been calculated, using the Jason-2 NRCS as the reference Ku band value. Figure 7 shows the extrapolated and actual Ka band NRCS using the Jason2 as a reference data as a function of wind speed for different values of the SWH. An excellent agreement is found at moderate and large wind speed (above 4 m/s) with less than 0.25 dB relative error while a more important discrepancy (up to 2 dB) is observed at small wind speeds. This deterioration of the prediction is consistent with the limitations of the GO4 model, which is not expected to hold at the smallest wind speeds.

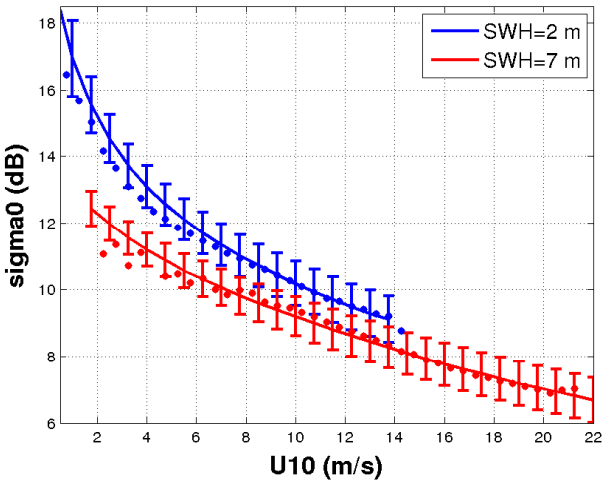



**Fig. 7:** AltiKa data (dots) and predicted bounds (solid lines with error bars) for the Ka band NRCS using Jason-2 reference data for SWH= 2 m (blue plots) and 7 m (red plots).

## VI. Conclusions

In this work we have made a systematic investigation of the variations of the Ku- and Ka-band backscatter from the sea surface with different oceanic parameters. For this we used one full year of AltiKa and Jason-2 altimeter data reprocessed with the same improved re-tracking method, namely IceNew. We proposed a simple Ku/Ka band extrapolation scheme based on the GO4 scattering model to assess the consistency of the two sets of data. We found that the Ka band NRCS has an increased sensitivity (when compared to the conventional Ku band) to wind speed and significant wave height. In addition, it has a non-negligible dependence on sea surface temperature, contrarily to the Ku band. The long waves or swells have a significant impact on the level of NRCS, for the same wind speed. Based on the GO2/GO4 model a simple expression could be obtained for the variation of NRCS induced by swell in terms of long wave mss. From this we have derived an elementary empirical relationship between the long wave mss and the SWH which can be used to improve Cox and Munk relation. At last we compared the Ku/Ka band extrapolation scheme derived from the GO4 with the actual Jason-2/AltiKa data and showed that this extrapolation is consistent with the model prediction except at very small wind speeds.

**Acknowledgments:** this work has been realized under the financial support of CNES (Etude R-S14/OT-0003-056).

## References

[1] J. Verron, P. Sengenes, J. Lambin, J. Noubel, N. Steunou, A. Guillot, N. Picot, S. Coutin-Faye, R. Sharma, RM Gairola, et al. The SARAL/Altika altimetry satellite mission. Marine Geodesy, 38(sup1):2–21, 2015.

[2] The SARAL/AltiKa Satellite Altimetry Mission, volume 38 of Marine Geodesy. Taylor and Francis, 2015.

[3] J Lillibridge, R Scharroo, S Abdalla, and D Vandemark. One- and two-dimensional wind speed models for ka-band altimetry. Journal of Atmospheric and Oceanic Technology, 31(3):630–638, 2014.

[4] S Abdalla. Calibration of Saral/Altika wind speed. IEEE Geoscience and Remote Sensing Letters, 11(6):1121–1123, 2014.

[5] G. D. Quartly. Metocean comparisons of Jason-2 and Altikaa method to develop a new wind speed algorithm. Marine Geodesy, 38(sup1):437–448, 2015.

[6] S. Abdalla. SARAL/AltiKa wind and wave products: monitoring, validation and assimilation. Marine Geodesy, 38(sup1):365–380, 2015.

[7] P. Prandi, S. Philipps, V. Pignot, and N. Picot. SARAL/AltiKa global statistical assessment and cross-calibration with Jason-2. Marine Geodesy, 38(sup1):297–312, 2015.

[8] U.M. Kumar, S.K. Sasamal, D. Swain, N. N. Reddy, and T. Ramanjappa. Intercomparison of geophysical parameters from SARAL/Altika and Jason-2 altimeters. IEEE Journal of Selected Topics in Applied Earth Observations and Remote Sensing, 8(10):4863–4870, 2015.

[9] H. Palanisamy, A. Cazenave, O. Henry, P. Prandi, and B. Meyssignac. Sea-level variations measured by the new altimetry mission saral/altika and its validation based on spatial patterns and temporal curves using jason-2, tide gauge data and an overview of the annual sea level budget. Marine Geodesy, 38(sup1):339–353, 2015.

[10] H. Sepulveda, P. Queffeulou, and F. Ardhuin. Assessment of SARAL/AltiKa wave height measurements relative to buoy, Jason-2, and cryosat-2 data. Marine Geodesy, 38(sup1):449–465, 2015.

[11] O Boisot, S Pioch, C Fatras, G Caulliez, A Bringer, P Borderies, J-C Lalaurie, and C-A Guérin. Ka-band backscattering from water surface at small incidence: A wind-wave tank study. Journal of Geophysical Research: Oceans, 120(5):3261–3285, 2015.

[12] O Boisot, F Nouguier, B Chapron, and C-A Guérin. The GO4 Model in Near-Nadir Microwave Scattering From the Sea Surface. IEEE Transactions on Geoscience and Remote Sensing, 53(11):5889–5900, 2015.

[13] F. Nouguier, A. Mouche, N. Rascle, B. Chapron, and D. Vandemark. Analysis of dual-frequency ocean backscatter measurements at Ku- and Ka-bands using near-nadir incidence GPM radar data. IEEE Geoscience and Remote Sensing Letters, 13(9):1310–1314, 2016.

[14] L. Amarouche, P. Thibaut, O. Z. Zanife, J.-P. Dumont, P. Vincent, and N. Steunou. Improving the Jason-1 Ground Retracking to Better Account for Attitude Effects. Marine Geodesy, 27(1-2):171–197, 2004.

[15] G Brown. The average impulse response of a rough surface and its applications. IEEE Transactions on Antennas and Propagation, 25(1):67–74, 1977.

[16] G Hayne. Radar altimeter mean return waveforms from near-normal-incidence ocean surface scattering. IEEE Transactions on Antennas and Propagation, 28(5):687–692, 1980.

[17] P. Thibaut, J-C. Poisson, E. Bronner, and N. Picot. Relative Performance of the MLE3 and MLE4 Retracking Algorithms on Jason-2 Altimeter Waveforms. Marine Geodesy, 33(sup1):317–335, 2010.

[18] Graham D Quartly. Optimizing $\sigma^0$ information from the Jason-2 altimeter. IEEE Geoscience and Remote Sensing Letters, 6(3):398–402, 2009.

[19] OSTM/Jason-2 Products Handbook. http://www.ospo.noaa.gov/Products/documents/J2_handbook_v1-8_no_rev.pdf, 2011.

[20] F Mercier, V Rosmorduc, L Carrere, and P Thibaut. Coastal and hydrology altimetry product (pistach) handbook. Technical report, Centre National d'Études Spatiales (CNES), Paris, France, http://www.aviso.altimetry.fr/fileadmin/documents/data/tools/hdbk_Pistach.pdf, 2010.

[21] AVISO. Peachi. Technical report, CNES, http://aviso.altimetry.fr/index.php?id=3116, 2013.

[22] G. Valladeau, P. Thibaut, B. Picard, J.-C. Poisson, N. Tran, N. Picot, and A. Guillot. Using Saral/Altika to improve ka-band altimeter measurements for coastal zones, hydrology and ice: The PEACHI prototype. Marine Geodesy, 38(sup1):124–142, 2015.

[23] J. Lambin, R. Morrow, L.-L. Fu, J. K. Willis, H. Bonekamp, J. Lillibridge, J. Perbos, G. Zaouche, P. Vaze, W. Bannoura, F. Parisot, E. Thouvenot, S. Coutin-Faye, E. Lindstrom, and M. Mignogno. The OSTM/Jason-2 mission. Marine Geodesy, 33(sup1):4–25, 2010.

[24] E Bronner, Ashok K. Shukla, N. Picot, A. Guillot, J.P. Dumont, V. Rosmorduc, J. Lillibridge, S. Desai, H. Bonekamp, R. Scharroo, and J. Figa. SARAL / AltiKa Products Handbook. 2013.

[25] Tanos Elfouhaily, Douglas Vandemark, Jérôme Gourrion, and Bertrand Chapron. Estimation of wind stress using dual-frequency topex data. Journal of Geophysical Research: Oceans, 103(C11):25101–25108, 1998.

[26] Graham D Quartly, Meric A Srokosz, and Trevor H Guymer. Global precipitation statistics from dual-frequency topex altimetry. Journal of Geophysical Research: Atmospheres, 104(D24):31489–31516, 1999.

[27] J Gourrion, D Vandemark, S Bailey, B Chapron, GP Gommenginger, PG Challenor, and MA Srokosz. A two-parameter wind speed algorithm for ku-band altimeters. Journal of Atmospheric and Oceanic technology, 19(12):2030–2048, 2002.

[28] D. Vandemark, B. Chapron, H. Feng, and A. Mouche. Sea surface reflectivity variation with ocean temperature at ka-band observed using near-nadir satellite radar data. IEEE Geoscience and Remote Sensing Letters, 13(4):510–514, 2016.

[29] R. W. Reynolds, T. M. Smith, C. Liu, D. B Chelton, K. S Casey, and M. G. Schlax. Daily High-Resolution Blended Analyses for Sea Surface Temperature. Journal of Climate, 20:5473–5496, 2007.

[30] C. Cox and W. Munk. Statistics from the sea surface derived from the sun glitter. J. Marine Res., 13:198–227, 1954.

[31] T. Meissner and F. J. Wentz. The complex dielectric constant of pure and sea water from microwave satellite observations. IEEE Transactions on Geoscience and Remote Sensing, 42(9):1836–1849, 2004.